Journal of Asian Earth Sciences: X 10 (2023) 100156

Contents lists available at ScienceDirect

Journal of Asian Earth Sciences: X

journal homepage: www.sciencedirect.com/journal/journal-of-asian-earth-sciences-x

Geochemistry of the Turonian-Coniacian strata: New insight into paleoenvironmental conditions of the Tethys, Eastern Pontides, NE Türkiye

Merve Özyurt [a,*], Raif Kandemir [b], Selim Yıldızoğlu [b]

[a] Department of Geological Engineering, Karadeniz Technical University, TR 61080 Trabzon, Türkiye
[b] Department of Geological Engineering, Recep Tayyip Erdogan University, TR-53100 Rize, Türkiye

ARTICLE INFO

Keywords:
Late Cretaceous
Eastern Pontide
Geochemistry
Sakarya Zone
NE Turkey
Ocean Anoxia
OAE
Climate conditions

ABSTRACT

The eastern part of the Sakarya Zone, known as the Eastern Pontides, is represented by a south-facing carbonate platform during the Late Jurassic-Early Cretaceous. The shallow marine carbonate sedimentation is masked by hemipelagic sedimentation during the Turonian to Coniacian. The Turonian-Coniacian strata are widely exposed in the Gümüşhane area. In this study, we present new microfacies and geochemical data that can provide new insights into the palaeo-oceanic conditions during the time of their deposition.

These strata consist of yellow to gray, thick-bedded, graded calcarenites, calcilutite, pelagic limestone, and monogenic conglomerates. The dominant components are carbonate fragments, including dolomites and limestone, as well as allochthonous bioclasts. Volcanic rock fragments, quartz, cherts, and glauconites are also present, with their abundance varying along the section. The micritic component and planktonic fauna exhibit an increasing abundance in the upward direction, indicating a gradual deepening of the depositional environment. Hence, the analyzed samples can be interpreted as transgressive series deposited on slopes or the deep shelf basin.

Furthermore, these strata exhibit distinct V/(V+Ni) and Ni/Co ratios without a notable negative Ce anomaly, suggesting relatively oxygen-reduced conditions. They also show a slight enrichment in alkali elements (Rb and Cs) and post-transition elements (Ga), and LREE, indicating intense weathering. The Ga/Rb and K/Al values further support warm and humid Cretaceous conditions. Thus, the Turonian-Coniacian strata offer valuable information about ancient environments, climate conditions, and the basin evolution of the Tethys Ocean in the Eastern Black Sea region.

1. Introduction

The Eastern Pontides was characterized by an extensive, generally south-sloping, carbonate-dominated shelf during the Late Jurassic-Early Cretaceous (Görür, 1988). The Eastern Pontides experienced the equatorial-subequatorial paleoclimate and a relatively stable tectonic regime, which facilitated the deposition of the platform carbonates (Görür, 1988; Kırmacı, 1992; Kirmaci et al., 1996; Okay and Sahinturk, 1997; Tasli et al., 1999; Koçyiğit and Altiner, 2002; Koch et al., 2008; Özyurt et al., 2019a-c; 2020; 2022; Özyurt and Kırmacı, under review). Shallow marine conditions were present during the Oxfordian – Early Aptian (e.g., Pelin, 1977; Taslı, 1991; Kırmacı, 1992; Kirmaci et al., 1996; Koch et al., 2008; Kara-Gülbay et al., 2012; Kırmacı et al., 2018; Vincent et al., 2018; Özyurt et al., 2019a). However, these conditions ended during the Late Aptian-Albian extensional tectonic regime, and the basin slightly started to deepen, and the inner platform environment turned into a deep shelf environment (Özyurt and Hollis, 2019; Özyurt, 2019; Özyurt et al., 2019a-c). The deepening of the depositional environment continued into the late Albian, with Sponge spicule wackestone/mudstone microfacies deposited in an upper slope environment (Özyurt et al., 2022). Moreover, Taslı and Özsayar (1997) recorded Albian monogenic conglomerates and Neptunian dikes, proposing that platform drowning was initiated along with the early phases of rifting. The rise in sea level at the onset of the Turonian led to further basin deepening, and carbonate deposition was masked by calciclastic materials associated with pelagic fauna (Taslı and Özsayar, 1997; Chen et al., 2015). In the graben areas, particularly in the Pirahmet area, rudstone/wackestone including calcisphere and planktonic foraminifera

Abbreviations: OAE, Oceanic Anoxic Event.

* Corresponding author.
E-mail address: merveyildiz@ktu.edu.tr (M. Özyurt).

https://doi.org/10.1016/j.jaesx.2023.100156
Received 8 December 2022; Received in revised form 30 May 2023; Accepted 1 June 2023
Available online 22 June 2023

were deposited together with reworked carbonates such as monomictic conglomerates, carbonate breccias, and calcarenites. The appearance of such facies has been attributed to the accelerated subsidence of the platform and the subsequent drowning phase of the platform carbonates, and their age is well constrained as Turonian-Coniacian (Taslı and Özsayar, 1997; Eren and Tasli, 2002). The previous researchers propose that the deepening of the paleoenvironment in the Eastern Pontides may be related to extensional tectonics causing subsidence and subsequent flooding of the basin as well as a global sea-level rise during the Cenomanian/Turanian period (e.g. Taslı and Özsayar, 1997). However, the paleoenvironmental and paleoclimatic conditions accompanied by the drastic change have not been fully understood (Özyurt et al., 2020). Hence, a detailed geochemical investigation, combined with sedimentological analyses, is still needed. In this study, we focused on the geochemical characteristics of the Turonian-Coniacian facies to discuss the mechanisms and complicated processes that the basin experienced.

2. Geologic setting

Türkiye is one of the major components of the Alpine-Himalayan orogenic system and comprises four major tectonic blocks (Okay & Tüysüz, 1999; Fig. 1). The study area is located in the eastern part of the Pontides tectonic unit, in northeastern Türkiye, around the city of Gümüşhane (Fig. 1). There is a heterogeneous pre-Jurassic basement in the southern part of the Eastern Pontides, which contains Paleozoic massifs composed of granites and metamorphic rocks (Fig. 1), as well as Permo-Carboniferous shallow marine to terrigenous sedimentary rocks (Okay and Sahinturk, 1997).

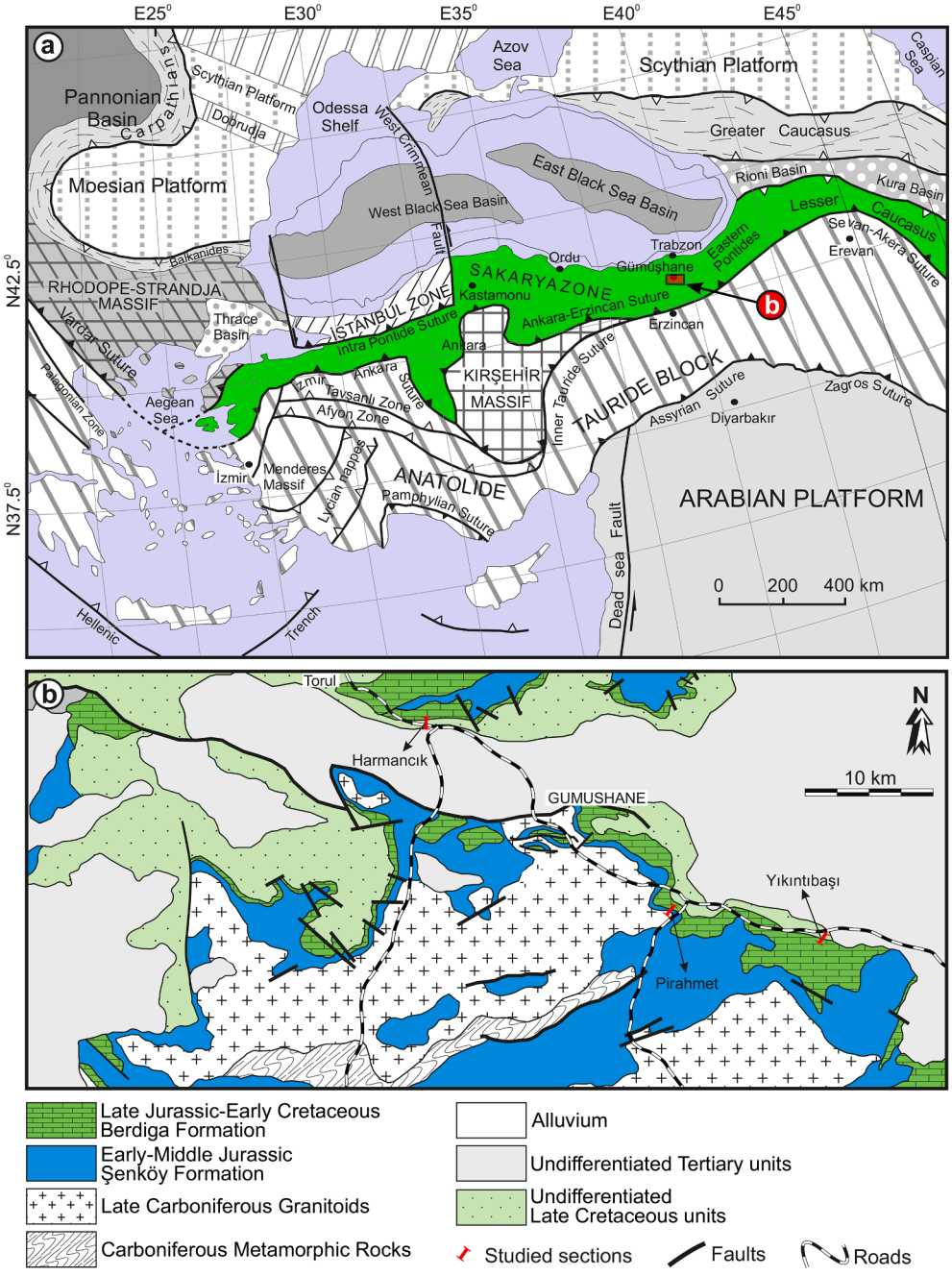

Fig. 1. (a) Regional tectonic setting of Türkiye (Okay and Tüysüz, 1999). (b) Simplified geological map of the Gümüşhane region and location of the investigated stratigraphic sections (modified from Güven, 1993).

The Lower-Middle Jurassic sequence unconformably overlies the heterogeneous pre-Jurassic basement rocks. The Early-Middle Jurassic sequence in the Eastern Pontides is predominantly represented by volcano-sedimentary formation (Şenköy Formation: Kandemir, 2004), which rests unconformably above the heterogeneous basement rocks. This sequence is characterized by rift-related sediments and exhibits significant differences in facies characteristics vertically and laterally (Kandemir, 2004; Kandemir et al., 2022). The Şenköy Formation is overlain by Upper Jurassic - Lower Cretaceous platform carbonates (Berdiga Formation: Pelin, 1977). The platform carbonates are represented by shallow marine facies, which change to the south into coeval deep marine facies, implying a south-facing carbonate platform of the Tethys Ocean.

The lower part of the platform carbonates consists of medium- to massive-bedded grey to yellowish oncolytic, intraclastic packstones and grainstones, and dolomites, which are changed into grainstones, packstones, and wackestone facies with rich benthic foraminiferal assemblages, fragments of mollusks, and echinoids, in parallel with the sedimentary evolution of the basin. In addition, chert nodules and planktonic fossils are abundantly present in the upper level of the carbonate sequence (Özyurt et al., 2020; 2022).

The lithostratigraphic succession of the southern part was very similar to the stratigraphic generation of the northern part until the Late Cretaceous. The generation of the Late Cretaceous and Middle Eocene

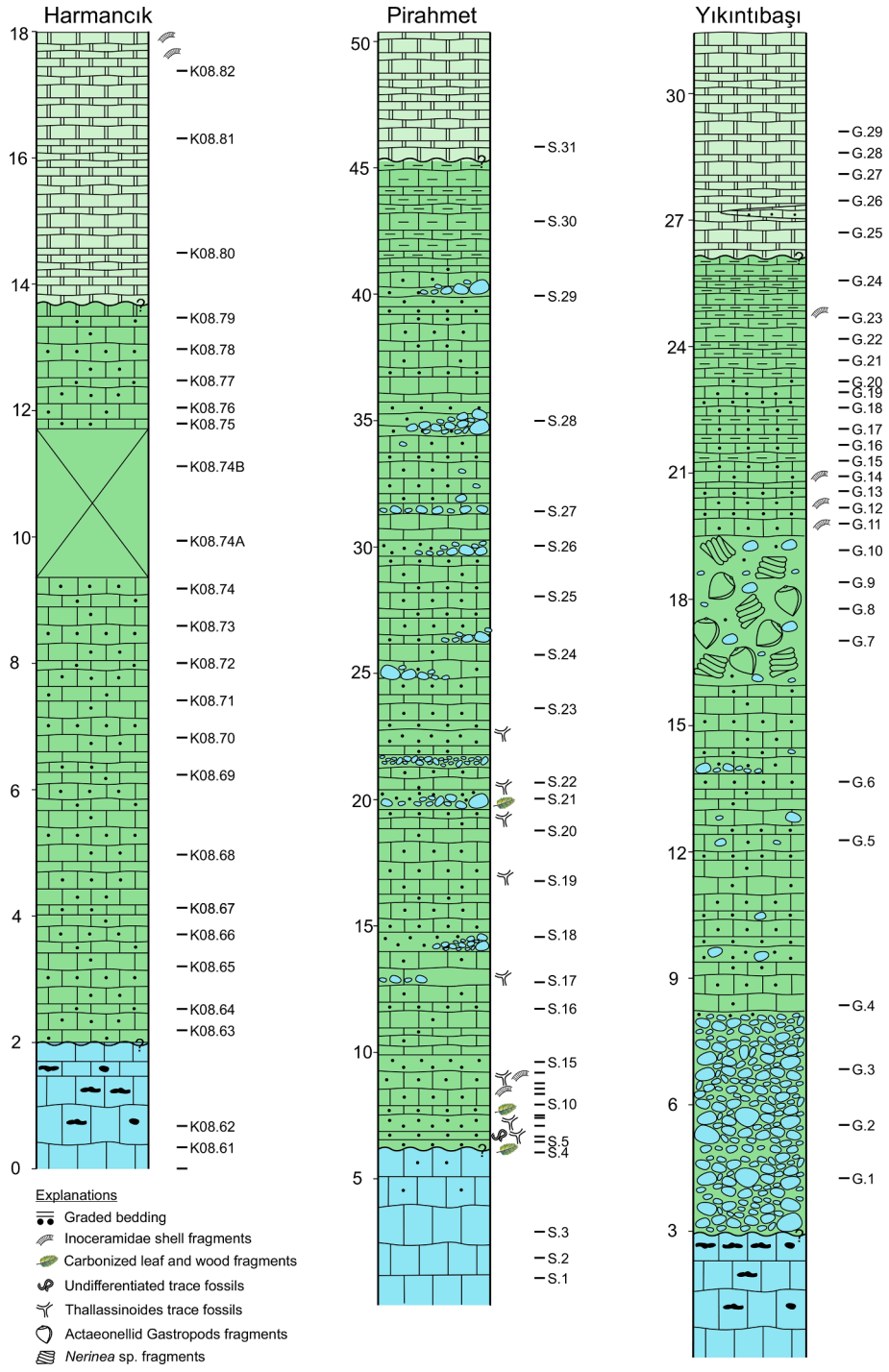

Fig. 2. Detailed stratigraphic sections of Turonian-Coniacian strata in the Gümüşhane region.

sequences results in lithostratigraphic differences between the southern and northern parts of the Eastern Pontides. The northern part of the Eastern Pontides is characterized by a volcano-sedimentary sequence up to 2 km thick (Okay and Sahinturk, 1997). However, in the southern part of the Eastern Pontides, the platform carbonates are overlain by Upper Cretaceous sedimentary rocks. The Cretaceous sedimentary rocks consist mostly of (i) yellowish calcirudite, calcarenite, calcilutite, sandy limestone, sandstone, and conglomerates, (ii) *Globotruncana*-bearing red pelagic limestones, marly limestone, mudstone, and (iii) a turbidite series with a minor amount of interbedded volcano-clastics including tuff layers (Pelin, 1977; Sari et al., 2014; Eyüboğlu, 2015; Türk-Öz and Özyurt, 2019). The Eocene Kabaköy Formation unconformably overlies the Late Cretaceous sedimentary units and other pre-Eocene units in the northern and southern zones of the Eastern Pontides. The Kabaköy

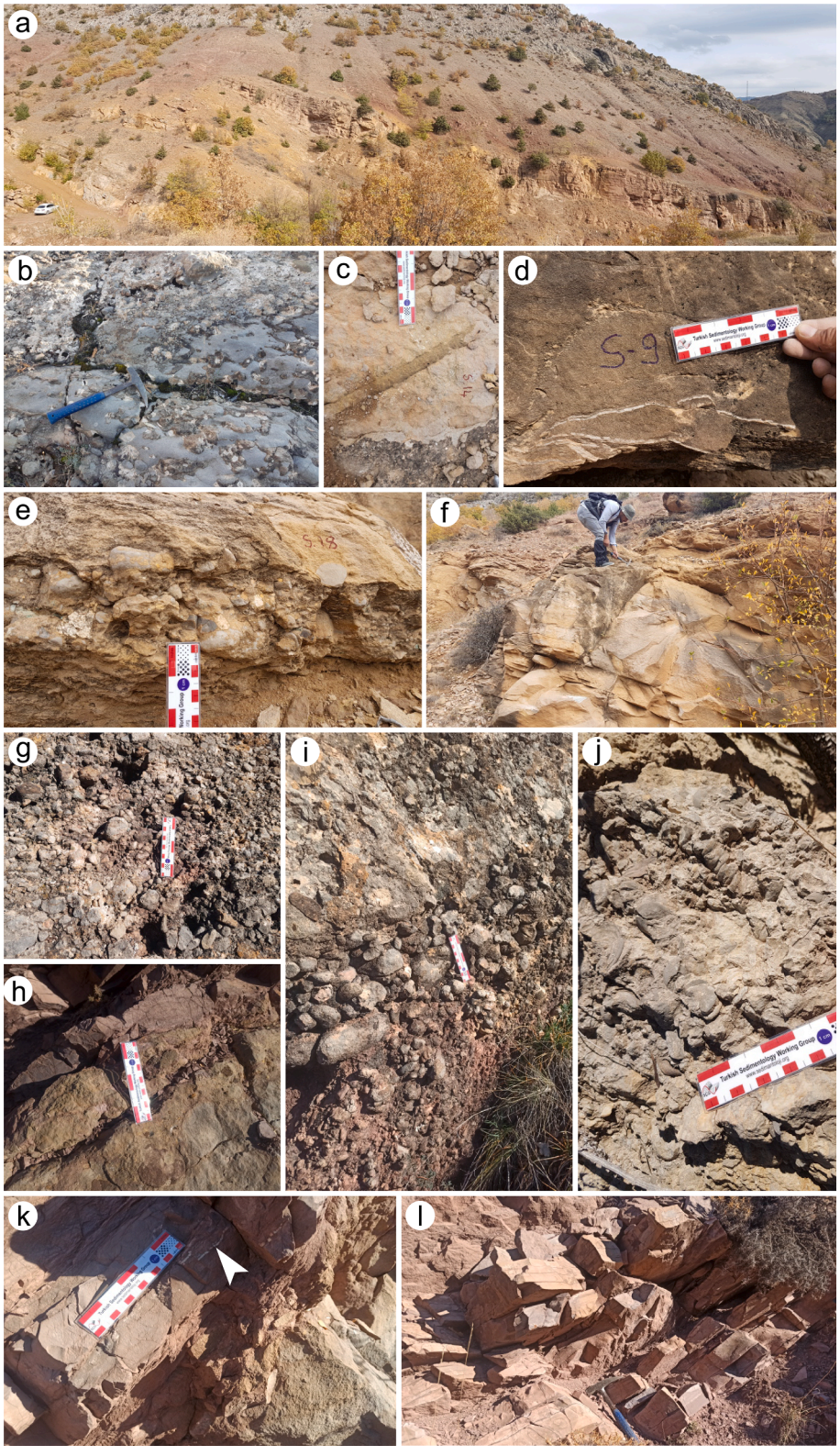

Fig. 3. General view of Turonian-Coniacian strata in three different measured stratigraphic sections. (a) View of the Turonian-Coniacian strata in the Pirahmet section (b) Cherty limestones on the top level of the platform carbonates (c) Trace fossils in the studied strata (d) Mollusc shell fragments at the base of the calcarenite beds (e) conglomeratic level in Pirahmet section (f) sandy limestone and calcarenite strata in the Pirahmet section (g-i) monogenic conglomerates in the Yıkıntıbaşı section (j) biostrom level consisting of Gastropods in the Yıkıntıbaşı section (k-l) *Globotruncana*-bearing red pelagic limestones. (For interpretation of the references to colour in this figure legend, the reader is referred to the web version of this article.)

Formation consists of andesite, basalt, and pyroclastics, with lesser amounts of sandstone, tuff, and sandy limestone, including Nummulites.

3. Methods

In this study, we focus on the Turonian-Coniacian strata in the Gümüşhane area. This study is based on three stratigraphic sections that were measured in Pirahmet, Harmancık, and Yıkıntıbaşı area in the Gümüşhane region (Fig. 1). Harmancık section is located between Gümüşhane and Torul roadway and Harmancık village, 10 km northwestern of Gümüşhane city center (Figs. 1 and 2). Yıkıntıbaşı section is located in Kale 1 km eastern of Gümüşhane city center (Figs. 1 and 2). The Pirahmet section is located in Pirahmet village 12 km south-eastern of Gümüşhane city center (Figs. 1 and 2) (Fig. 3a). Most representative samples were collected from three stratigraphic sections (Fig. 3a-l). 21 samples were collected from the 18 m thick Harmancık stratigraphic section, 31 samples from the 50 m thick Pirahmet stratigraphic section, and 29 samples from the 32 m thick Yıkıntıbaşı stratigraphic section. A total of 78 samples were petrographically analyzed under a polarized microscope (Fig. 4a-i). The geochemical analyses are based on the Pirahmet section. The petrographically least weathered and altered calc-litharenites and calcilutites were selected for trace element analyses.

The Major and trace element of each sample was carried out by ACME Analytical Laboratories, Ltd. (Vancouver, BC, Canada). Major element analyses have been conducted by ACME Analytical Laboratories, Ltd. (Vancouver, BC, Canada). The major element contents of the selected 8 samples were determined by inductively coupled plasma mass spectrometry (ICP-MS). The standard suite of major oxides which are defined in methods (ACME brochure-2017, 31 p) is analyzed at ACME Lab (Canada) for each sample. During the whole rock major analysis processes, STD SO-19 is used for Reference Materials. STD SO-19 has 2.91 % of MgO and 5.89 % of CaO. The detection limit is 0.01 and the upper limit is 100 % for CaO and MgO. Sample preparation (dissolving in acid and filtering) and measurements were conducted at ACME Analytical Laboratories Ltd. (Canada). Major element compositions were determined from pulps after 0.2 g samples of rock powder were fused with 1.5 g $LiBO_2$ and then dissolved in 100 mL 5% HNO_3. The samples were reduced to chips of 2–4 mm and pulverized in a

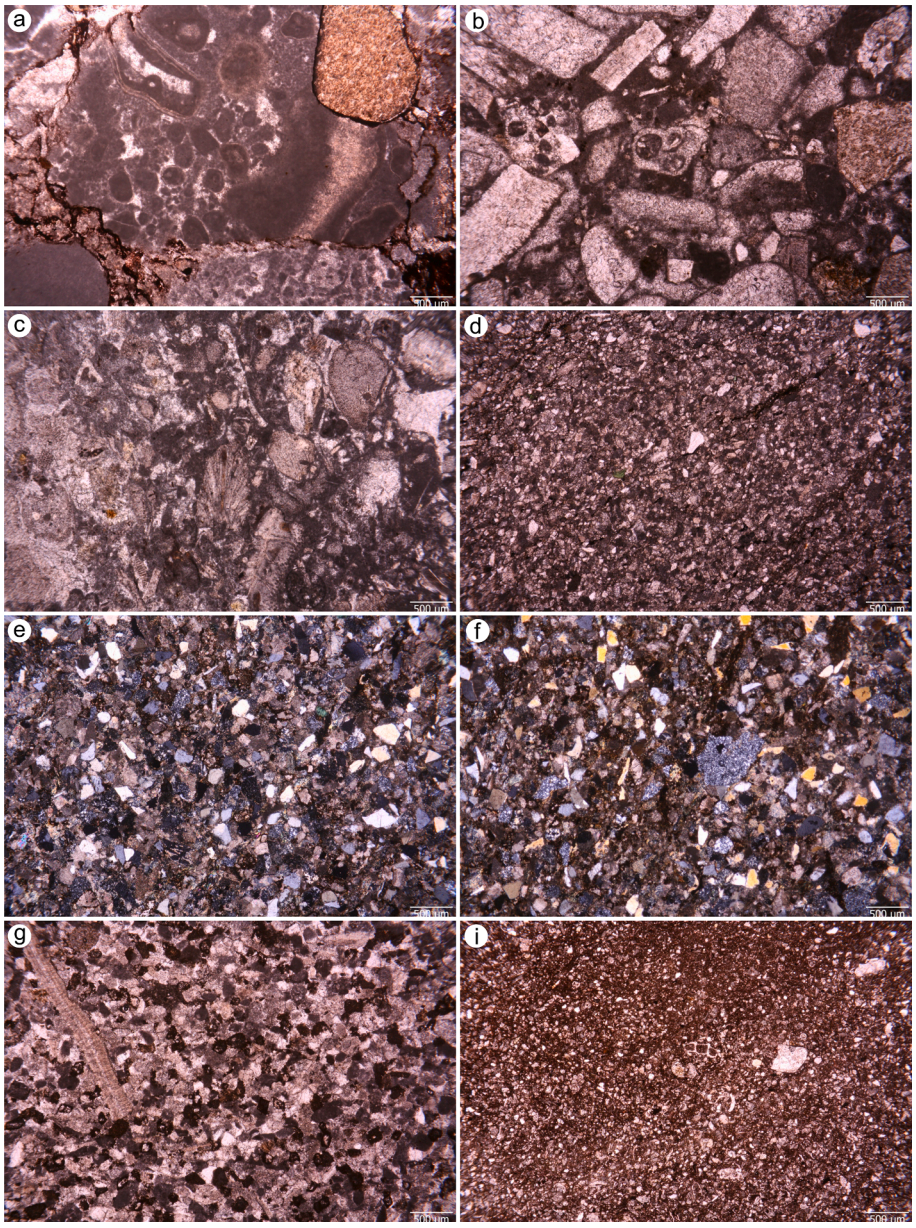

Fig. 4. Thin section images showing the representative facies characteristics of the studied samples. (a) The conglomerates with limestone fragment (G2 sample); (b) calc-litharenite with abundant carbonate component and allochthonous bioclasts (G8 sample); (c) calc-litharenite with allochthonous bioclasts and reworked carbonate component (K08-65 sample); (d) calc-litharenite to calcilutite with carbonate fragments and glauconite (S17 sample); (e) litharenite to calc-litharenite containing abundant poorly rounded-quartz, chert, and volcanic rock fragment and carbonate fragment (S-21 sample); (f) calc-litharenite containing abundant poorly rounded volcanic rock fragments, quartz, cherts and carbonate component (S5 sample); (g) calc-litharenite with reworked carbonate component and bivalve derived by nearby platform (S-30 sample) and (i) overlying pelagic limestone (S-31).

thoroughly cleaned agate ring mill to avoid contamination. 0.2 g aliquot of samples for the major element analysis were weighed into a graphite crucible and mixed with 1.50 g of $LiBO_2/Li_2B_4O_7$ flux and these were subjected to a temperature of 980 °C for thirty minutes. The residue was later dissolved in 5% HNO_3 (ACS-grade nitric acid diluted in distilled water). Replicate analyses show that errors for major elements vary between 1 and 2%. Analyses used ~0.2 g of powdered sample digested in 10 mL 8 N HNO_3, of which 1 mL was diluted with 8.8 mL deionized water and 0.1 mL HNO_3. To monitor the precision and accuracy, 1 mL of an internal standard (including Bi, Sc, and In) was added to the solution. For more details on these methods, please see the website of http://acmelab.com.

4. Results

4.1. Stratigraphic framework and sections

The best typical exposures of the formation are widely exposed in

Table 1
Major and trace element contents of the studied samples.

		S-5	S-10	S-17	S-19	S-23	S-25	S-30
Analyte		Rock Pulp	Rock Pulp	Rock Pulp	Rock Pulp	Rock Pulp	Rock Pulp	Rock Pulp
SiO_2	%	33.52	34.37	45.49	35.95	31.36	29.20	39.78
Al_2O_3	%	6.39	7.60	9.39	7.69	6.35	5.88	9.19
Fe_2O_3	%	2.45	3.05	3.46	2.94	2.93	2.05	1.90
MgO	%	4.49	6.73	3.48	7.34	3.69	2.08	2.83
CaO	%	24.43	20.06	15.49	18.37	26.33	30.76	21.24
Na_2O	%	0.03	0.03	0.04	0.03	0.03	0.03	0.03
K_2O	%	1.64	1.97	2.51	2.00	1.60	1.40	1.97
TiO_2	%	0.26	0.43	0.77	0.43	0.29	0.22	0.40
P_2O_5	%	0.04	0.06	0.07	0.06	0.04	0.04	0.06
MnO	%	0.05	0.04	0.03	0.04	0.05	0.05	0.03
Cr_2O_3	%	0.00	0.01	0.01	0.01	0.00	0.00	0.00
LOI	%	26.50	25.40	19.00	24.90	27.20	28.20	22.40
Sum	%	99.86	99.80	99.80	99.79	99.85	99.88	99.87
Ba	ppm	354.00	133.00	273.00	166.00	187.00	134.00	197.00
Sc	ppm	4.00	7.00	8.00	6.00	5.00	4.00	7.00
Co	ppm	1.80	3.10	10.40	3.80	2.30	1.70	4.10
Cs	ppm	0.70	1.20	1.10	1.20	0.70	0.80	1.10
Ga	ppm	4.90	6.70	8.10	6.90	5.40	4.40	7.30
Hf	ppm	2.90	4.50	10.50	4.70	2.90	3.10	3.30
Nb	ppm	3.00	5.00	7.80	5.00	3.10	2.50	4.20
Rb	ppm	28.90	32.80	39.90	33.60	26.10	26.20	33.80
Sr	ppm	262.00	302.10	266.90	287.90	363.10	431.90	291.20
Ta	ppm	0.20	0.20	0.40	0.30	0.20	0.10	0.30
Th	ppm	3.20	4.60	10.40	5.00	4.20	3.50	3.90
U	ppm	0.90	1.60	3.60	1.40	1.30	1.10	1.30
V	ppm	34.00	67.00	101.00	51.00	46.00	37.00	64.00
Zr	ppm	112.10	171.90	420.50	183.80	111.30	116.90	120.30
Y	ppm	12.60	18.00	21.10	14.80	14.90	13.90	12.20
La	ppm	11.90	16.70	33.20	16.80	15.50	11.10	15.00
Ce	ppm	20.60	28.80	57.10	30.50	28.50	20.60	27.80
Pr	ppm	2.29	3.39	6.17	3.43	3.11	2.25	3.13
Nd	ppm	9.30	12.30	22.40	12.90	12.30	8.70	11.50
Sm	ppm	1.69	2.49	4.34	2.45	2.34	1.82	2.38
Eu	ppm	0.53	0.62	0.89	0.58	0.67	0.61	0.63
Gd	ppm	1.93	2.52	3.92	2.34	2.45	2.27	2.13
Tb	ppm	0.31	0.43	0.63	0.35	0.40	0.36	0.34
Dy	ppm	1.86	2.79	3.83	2.22	2.49	2.12	2.07
Ho	ppm	0.40	0.68	0.80	0.46	0.51	0.46	0.45
Er	ppm	1.28	1.95	2.50	1.53	1.50	1.37	1.31
Tm	ppm	0.20	0.31	0.37	0.25	0.24	0.21	0.20
Yb	ppm	1.29	2.14	2.57	1.70	1.47	1.59	1.33
Lu	ppm	0.20	0.37	0.42	0.29	0.23	0.25	0.24
REE	ppm	53.78	75.49	139.14	75.80	71.71	53.71	68.51
LREE	ppm	48.24	66.82	128.02	69.00	64.87	47.35	62.57
HREE	ppm	5.54	8.67	11.12	6.80	6.84	6.36	5.94
Y/Ho		31.50	26.47	26.38	32.17	29.22	30.22	27.11
Eu/Eu*		0.89	0.75	0.64	0.73	0.85	0.91	0.84
Ce/Ce*		0.90	0.88	0.90	0.92	0.94	0.95	0.93
La/Yb_N		6.27	5.30	8.78	6.71	7.16	4.74	7.66
Pr/Yb_N		3.08	2.75	4.17	3.50	3.67	2.46	4.08
Nd/Yb_N		2.54	2.02	3.07	2.67	2.95	1.93	3.05
La/Sm_N		4.40	4.19	4.78	4.28	4.14	3.81	3.94
Th/U		3.56	2.88	2.89	3.57	3.23	3.18	3.00
Th/Sc		0.80	0.66	1.30	0.83	0.84	0.88	0.56
Ni/Co		0.94	0.65	1.09	0.58	0.87	1.35	0.73
La/Sc		2.98	2.39	4.15	2.80	3.10	2.78	2.14
Co/Th		0.56	0.67	1.00	0.76	0.55	0.49	1.05
Zr/Sc		28.03	24.56	52.56	30.63	22.26	29.23	17.19
Th/Co		1.78	1.48	1.00	1.32	1.83	2.06	0.95
La/Co		6.61	5.39	3.19	4.42	6.74	6.53	3.66
CIA		78.99	78.92	78.38	78.87	79.28	80.11	81.91
ICV		5.23	4.26	2.75	4.06	5.51	6.23	3.10

several locations of the Gümüşhane area. There different stratigraphic sections are measured in several localities including, Pirahmet, Harmancık, and Yıkıntıbaşı stratigraphic sections (Fig. 1). These stratigraphic sections can be well correlated with a typical section of Kındıralık Fm. that is named by Pelin (1977). We, here, present the main lithological and macro-sedimentological characteristics of three stratigraphic sections.

The thickness of the studied facies ranged from 5 m to 50 m (e.g. Taslı and Özsayar, 1997). The studied unit unconformably overlies the sponge spicule-bearing wackestone/mudstone facies of the Berdiga Formation. The studied unit are generally represented by yellow to gray, thick-bedded, graded, and locally bioturbated calc-arenites, limestone, and monogenic conglomerates (e.g. Yıldızoğlu, 2022). The most common components are carbonate fragments (dolomites and limestone) and allochthonous bioclast derived from nearby carbonate platforms (Özyurt et al, under review). They include echinoderm, coralline algae, pelecypods, bryozoa, sponge spicules, and infrequent benthic foraminifera such as *Gaudryina* sp. (e.g. Taslı and Özsayar, 1997). The wide range of volcanic rock fragments, quartz, cherts, and glauconites are also observed and their abundance shows differences along the section. They are represented by yellow to gray monogenic poorly sorted-bresh, red well-sorted grain/matrix-supported monogenic conglomerates, yellow sandy limestone, calc-litharenites, and sandstone. The monogenic conglomerates are grain-supported with a small amount of matrix including benthic and pelagic foraminifers (e.g. Yilmaz and Kandemir, 2006). They gradually evolve into calc-litharenites or calciturbidites. The calciturbidites commonly are represented by normally-graded wackestones and packstones containing allochthonous bioclasts such as small benthic foraminifers, echinoderms, bryozoans, and pelagic foraminifers and sand-sized lithoclasts (Yilmaz and Kandemir, 2006). The calciturbites gradually turn into pelagic limestone or marl layers upwardly. The planktonic foraminifera is recorded in the upper part of the calciturbites (Taslı and Özsayar, 1997). Moreover, Taslı and Özsayar (1997) assigned the so-called calcarenites (the studied strata), which unconformably overlie different stratigraphic levels of the underlying platform carbonates (Berdiga Formation), to the Turonian-Coniacian based on the presence of *Helvetoglobotruncana*, *Marginotruncana*, and *Dicarinella* in the conformably overlying and/or intercalated pelagic limestone.

4.2. Geochemistry

Major and trace element results are illustrated in Table 1. The studied samples are represented by Al_2O_3/SiO_2 (0,19–0,23; ave. of 0,21), K_2O/Na_2O (46,67–62,75; ave. of 59,50), Fe_2O_3 + MgO (4,13–10,28; ave. of 7,06), TiO_2 (0,22–0,77; ave. of 0,40) and low SiO_2 (29,20–45,49, with an average of 35,67) values. Their V/Ni, V/(V + Ni), and U/Th ratios vary from 8.94 to 33.50, 0.90–0.97, and 0.28–0.35, respectively. They have high Sr/Cu (38.13 to 218.33) and K/Al values (0.21 to 0.27). Their Rb/Sr (0.06 to 0.15) and Sr/Ba (0.74 to 3.22) are relatively low. Their average ∑REE contents are lower than the average ∑REE contents of PAAS (183.0 ppm) and UCC (146.4 ppm) (Taylor and McLennan, 1985). Their PAAS-normalized REE patterns display (i) slight depletion LREE compared to HREE with high La/Yb_N ratios (0.47 to 0.87 with average 0.66) and, (ii) flat to slight positive Eu/Eu* anomaly (1.15 to 1.57 with average 1.40), and (iii) relatively flat Ce/Ce* (0.92 to 0.99 with average 0.96). They have varied La/La* (1.09–1.50; ave. 1.23), Gd/Gd* (0.99–1.21; ave. 0.07), and Pr/Pr* (0.93–1.02; ave. 0.97).

5. Discussion

5.1. Redox

The distribution of trace elements such as Fe, V, Mo, Ni, Mn, U, Th, Ce, and Cr in sediments are useful indicators of the redox conditions of the water column during sedimentation, as demonstrated by several studies (Galarraga et al., 2008; Qin et al., 2022). The U/Th ratio is often used as an indicator of marine anoxia or euxinia, where higher values suggest oxygen-depleted conditions. This ratio reflects the scavenging and preservation of uranium under reducing conditions, and its enrichment relative to thorium indicates limited oxygen availability (Zatoń et al., 2009). However, the U/Th ratio in carbonate-bearing rocks can be affected by uranium mobility during diagenesis, which can lead to post-depositional alteration and unreliable interpretations of redox conditions. It's important to consider other geochemical parameters and corroborating evidence to ensure an accurate interpretation of redox conditions. V and Ni ratios are particularly useful in this regard (Quinby-Hunt and Wilde, 1994; Galarraga et al., 2008; Yandoka et al., 2015). The V/Ni ratios are commonly used to interpret redox conditions, with ratios greater than 3.0 and ratios between 1.9 and 3.0 suggesting reducing and suboxic conditions, respectively (Galarraga et al., 2008). Similarly, ratios of V/(V+Ni) greater than 0.84, between 0.54 and 0.82, and between 0.46 and 0.60 indicate euxinic, anoxic, and dysoxic conditions, respectively (Pan et al., 2022). The V/Ni and V/(V+Ni) ratios suggest suboxic to dysoxic conditions, with average ratios of 2.3 and 0.7 (as shown in Table 1). In addition, the PAAS (Post-Archean Australian Shale) normalized cerium (Ce) anomaly is a commonly used indice to assess redox conditions (Bau, 1999; Özyurt et al., 2020). The cerium exists in two oxidation states (Ce^{3+} and Ce^{4+}) in marine systems. The oxygen-reduced conditions can lead to Ce^{3+} oxidation to insoluble Ce^{4+} and the partial scavenging of dissolved Ce^{3+} from seawater in anoxic marine systems (Bau and Alexander, 2006). As a result, the lack of significant negative-Ce anomalies in marine sediments has been considered evidence of oxygen-depleted conditions. The studied samples (particularly those from the lower part of the section) display relatively high Ce/Ce* values, which can support suboxic environments during the deposition of the studied strata (e.g. Özyurt and Hollis, 2019).

5.2. Paleoclimate

Paleoclimate plays a significant role in sediment mineralogy and geochemistry. Weathering processes are closely linked to climate, with warm and humid climates promoting intense chemical weathering, while cold and arid climates result in minimal chemical weathering (Nesbitt et al., 1996). The Ga/Rb ratio, which represents the ratio of gallium to rubidium, can serve as an indicator of weathering intensity. Several studies (e.g., Johnsson and Basu, 1993; Wang et al., 1997; Beckmann et al., 2005; Fathy et al., 2018) have shown that sedimentary ratios such as Ga/Rb, K/Al, Sr/Cu, and Rb/Sr are sensitive indicators of climatic variations during deposition.

A Sr/Cu ratio between 1.3 and 5.0 is indicative of a humid environment, while a ratio greater than 5.0 suggests aridity (e.g. Adegoke et al., 2014; Sarki Yandoka et al., 2015). Additionally, Rb/Sr ratios generally decrease with increasing aridity (e.g. Deng and Qian, 1993; Roy and Roser, 2013). However, caution should be exercised when applying these ratios to calciturbites due to potential Sr incorporation in the carbonate component. Sr tends to substitute for Ca in the crystal lattice due to their similar sizes and charges. The analyzed rocks encompass a wide range of carbonate components, leading to variable Sr concentrations, which can complicate the interpretation of Sr/Cu and Rb/Sr ratios. Therefore, alternative proxies or complementary geochemical indices may be more suitable for assessing paleoenvironmental conditions.

Humid climates enhance chemical weathering processes, which play a crucial role in the dissolution and transport of elements, including gallium and rubidium. In such environments, gallium is more prone to leaching and removal, resulting in an increased input of Ga to the marine system. Gallium and rubidium can exhibit different behaviors due to their differences in solubility and mobility, leading to their relative enrichment during weathering processes. Conversely, drier environments typically experience reduced chemical weathering, resulting in lower gallium concentrations relative to rubidium. Therefore, higher Ga/Rb ratios in sedimentary rocks indicate more intense weathering

under humid conditions, while lower Ga/Rb ratios are associated with less intense weathering in arid climates (e.g. Roy and Roser, 2013). Similarly, low K/Al ratios in sediments are indicative of a warm and humid climate during their formation, reflecting the enhanced chemical weathering, leaching, and transportation of elements, particularly K, under these conditions (e.g. Nesbitt and Young, 1982). The studied samples show low K/Al ratios, suggesting a warm and humid climate during their formation. This interpretation is supported by the enrichment of LREE values compared to underlying strata, as reported in the study by Özyurt et al. (2020). The elevated concentrations of these elements can be attributed to the increased mobility of LREEs under humid conditions, leading to their release from primary minerals and subsequent transportation to basins through weathering processes. However, it is important to note that the behavior of REEs under humid conditions is complex and can be influenced by various factors (Piper, 1974; Özyurt et al., 2020).

5.3. Depositional environment

The invasion of pelagic conditions has accelerated during the Turonian Coniacian. The shallow marine carbonates have been replaced by re-deposited carbonates. The sedimentation varies between calciturbites and hemipelagic limestone. They are mostly represented by calciturbites, monogenic conglomerates, and pelagic limestones. The calciturbites are locally interfingered with sandstone, displaying significant changes in lithology and thickness. The presence of *Globotruncana* and a micritic matrix within the fine-grained calcarenites suggests a slope environment (Taslı and Özsayar, 1997). Reworked fossil assemblages, such as coralline algae, bryozoa, and echinoids, imply the presence of some isolated platforms remaining within the photic zone or partial drowning. It has been reported a gradual decrease in sediment size and an association with benthic foraminifera, including T*extularia* and *Valvulina* (Kılıç, 2009). In addition, the micritic component and planktonic fauna show an increasing abundance upwardly, implying a gradual deepening of the depositional environment. The deepening of the basin has continued until the deposition of red *Globotruncana*-bearing pelagic limestones (Eren and Tasli, 2002; Kılıç, 2009; Türk-Öz and Özyurt, 2019).

5.4. Background controls

The Cenomanian/Turonian period is known for the occurrence of Oceanic Anoxic Event 2 (OAE 2) (Schlanger and Jenkyns, 1976). The OAE 2 has caused significant chemical changes in the Mesozoic Ocean (Jenkyns, 2010; Wagreich, 2012). The change in the faunal and floral association is widely interpreted as the result of oxygen-depleted conditions (Arthur et al., 1987; Jarvis et al., 1988; Hilbrecht, 1997; Zhang et al., 2016). Similarly, our sedimentologic analyses, combined with previous paleontological and stratigraphic approaches in the Eastern Pontides (Taslı and Özsayar, 1997; Kırmacı et al., 1996), confirm an important change in sedimentological patterns in the Eastern Pontides. Geochemical indices, such as V/(V + Ni) and Ni/Co, imply that the redox conditions of the basin during the deposition of the studied strata were mostly suboxic conditions (Algeo and Maynard, 2004; Tribovillard et al., 2006; Wang et al., 2018). These findings raise questions regarding the possible relationship between the influence of the global anoxic event and the initiation of drowning (e.g. Özyurt et al., in prep.). Alternatively, the drowning of the platform in the Eastern Pontides could be attributed to the relative subsidence caused by either local or global tectonic movements, as evidenced by the presence of Neptunian dikes and carbonate breccia (Taslı and Özsayar (1997). Similar patterns can be observed in the western Pontides as well (Masse et al., 2009; Yilmaz et al., 2010; Tüysüz, 2018).

On the other hand, various researchers have indicated that the sea level during the Cenomanian/earliest Turonian stage was exceptionally high and is considered one of the highest sea-level stands (e.g. Hancock & Kauffman, 1979; Haq et al. 1987, and Haq, 2014). This stage also witnessed the highest ocean water temperatures, occasionally interrupted by relatively cooler intervals (Hu et al. 2012; Forster et al., 2007; Jarvis et al, 2015). Similarly, warm climate conditions with climatic fluctuations were also recorded in Turonian–Coniacian sediments (Northwest Caucasus) (Yakovishina et al., 2022). Our paleoclimate indices confirm warm and humid conditions. Thus, our results have the potential to contribute new information on palaeoceanic conditions in the Tethys Ocean in the Eastern Pontides, Eastern Black Sea region. However, the background factors influencing the drowning event can vary and may involve a combination of different processes such as variations in eustatic sea-level rise, tectonic subsidence, changes in climate and environmental conditions, and/or local geological parameters. Thus it is necessary to conduct further research in the Eastern Pontides, Black Sea region, to better understand the dynamics of the Cenomanian to Coniacian strata and the role of OAE 2 in the drowning event.

6. Conclusion

The new microfacies and geochemical data provide valuable insights into the understanding of paleoenvironmental conditions and depositional settings for the studied sedimentary succession. These findings can be summarized as follows:

- The studied samples can be considered as transgressive series, displaying a predominantly continental slope environment.
- The V/Ni, V/(V+Ni), and Ce/Ce* ratios suggest suboxic environments during the deposition of the studied strata. This indicates relatively low oxygen levels in the depositional setting.
- Our paleoclimate indices, such as Ga/Rb and K/Al, mostly support warm and humid conditions during the deposition of the studied strata.
- The sedimentological and geochemical findings can suggest that the initiation of drowning can be linked to the consequences of OAE 2 (Oceanic Anoxic Event 2). Therefore, it is recommended to conduct high-resolution studies focusing on the Cenomanian to Coniacian strata in the Eastern Pontides, Black Sea region, to further investigate this phenomenon.

CRediT authorship contribution statement

Merve Özyurt: Conceptualization, Writing – original draft. **Raif Kandemir:** Supervision, Writing – review & editing. **Selim Yıldızoğlu:** Conceptualization.

Declaration of Competing Interest

The authors declare that they have no known competing financial interests or personal relationships that could have appeared to influence the work reported in this paper.

Data availability

Data will be made available on request.

Acknowledgment

This work is part of Selim Yıldızoğlu's MS thesis at Recep Tayyip Erdogan University. Special thanks to Nurbanu Ergül, Ali Keskin, and other internship students from Karadeniz Technical University for their help during the geological field and laboratory work. Appreciation is extended to Prof. Dr. Bilal Sarı (Dokuz Eylül University) and Prof. Dr. Kemal Taslı (Mersin University) for their assistance in paleontological and petrographical studies. Special thanks are also due to Editor Prof. Dr. İbrahim Uysal, Prof. Dr. Cüneyt Şen, and the reviewers for their

efforts in improving our paper.

References

Adegoke, A.K., Abdullah, W.H., Hakimi, M.H., Yandoka, B.M.S., 2014. Geochemical characterisation of Fika Formation in the Chad (Bornu) Basin, northeastern Nigeria: implications for depositional environment and tectonic setting. Appl. Geochem. 43, 1–12.

Algeo, T.J., Maynard, J.B., 2004. Trace-element behavior and redox facies in core shales of Upper Pennsylvanian Kansas-type cyclothems. Chem. Geol. 206 (3–4), 289–318.

Arthur, M.A., Schlanger, S.T., Jenkyns, H.C., 1987. The Cenomanian-Turonian Oceanic Anoxic Event, II. Palaeoceanographic controls on organic-matter production and preservation. Geol. Soc. Lond. Spec. Publ. 26 (1), 401–420.

Bau, M., 1999. Scavenging of dissolved yttrium and rare earths by precipitating iron oxyhydroxide: experimental evidence for Ce oxidation, Y-Ho fractionation, and lanthanide tetrad effect. Geochim. Cosmochim. Acta 63 (1), 67–77.

Bau, M., Alexander, B., 2006. Preservation of primary REE patterns without Ce anomaly during dolomitization of Mid-Paleoproterozoic limestone and the potential re-establishment of marine anoxia immediately after the "Great Oxidation Event". S. Afr. J. Geol. 109 (1–2), 81–86.

Beckmann, B., Flögel, S., Hofmann, P., Schulz, M., Wagner, T., 2005. Orbital forcing of Cretaceous river discharge in tropical Africa and ocean response. Nature 437 (7056), 241–244.

Chen, X., Wang, C., Wu, H., Kuhnt, W., Jia, J., Holbourn, A., Ma, C., 2015. Orbitally forced sea-level changes in the upper Turonian–lower Coniacian of the Tethyan Himalaya, southern Tibet. Cretac. Res. 56, 691–701.

Deng, H.W., Qian, K., 1993. Sedimentary geochemistry and environmental analysis. Gansu Science and Technology Press, Lanzhou, China, pp. 30–50.

Eren, M., Tasli, K., 2002. Kilop cretaceous hardground (Kale, Gümüshane, NE Turkey): description and origin. J. Asian Earth Sci. 20 (5), 433–448.

Eyuboglu, Y., 2015. Petrogenesis and U–Pb zircon chronology of felsic tuffs interbedded with turbidites (Eastern Pontides Orogenic Belt, NE Turkey): Implications for Mesozoic geodynamic evolution of the eastern Mediterranean region and accumulation rates of turbidite sequences. Lithos 212, 74–92.

Fathy, D., Wagreich, M., Gier, S., Mohamed, R.S., Zaki, R., El Nady, M.M., 2018. Maastrichtian oil shale deposition on the southern Tethys margin, Egypt: Insights into greenhouse climate and paleoceanography. Palaeogeogr. Palaeoclimatol. Palaeoecol. 505, 18–32.

Forster, A., Schouten, S., Baas, M., Sinninghe Damsté, J.S., 2007. Mid-Cretaceous (Albian–Santonian) sea surface temperature record of the tropical Atlantic Ocean. Geology 35 (10), 919–922.

Galarraga, F., Reategui, K., Martïnez, A., Martínez, M., Llamas, J.F., Márquez, G., 2008. V/Ni ratio as a parameter in palaeoenvironmental characterisation of nonmature medium-crude oils from several Latin American basins. J. Pet. Sci. Eng. 61 (1), 9–14.

Görür, N., 1988. Timing of opening of the Black Sea basin. Tectonophysics 147 (3–4), 247–262.

Güven, İ.H., 1993 1:25000 Scale Geology and Compilation of the Eastern Pontide: General Directorate of Mineral Research and Exploration of Turkey, Ankara (unpublished).

Hancock, J.M., Kauffman, E.G., 1979. The great transgressions of the Late Cretaceous. J. Geol. Soc. London 136 (2), 175–186.

Haq, B.U., 2014. Cretaceous eustasy revisited. Global Planet. Change 113, 44–58.

Haq, B.U., Hardenbol, J.A.N., Vail, P.R., 1987. Chronology of fluctuating sea levels since the Triassic. Science 235 (4793), 1156–1167.

Hilbrecht, H., 1997. Morphologic gradation and ecology in Neogloboquadrina pachyderma and N. dutertrei (planktic foraminifera) from core top sediments. Mar. Micropaleontol. 31 (1–2), 31–43.

Hu, X., Wagreich, M., Yilmaz, I.O., 2012. Marine rapid environmental/climatic change in the Cretaceous greenhouse world. Cretac. Res. 38, 1–6.

Jarvis, I., Carson, G.A., Cooper, M.K.E., Hart, M.B., Leary, P.N., Tocher, B.A., Rosenfeld, A., 1988. Microfossil assemblages and the Cenomanian-Turonian (Late Cretaceous) oceanic anoxic event. Cretac. Res. 9 (1), 3–103.

Jarvis, I., Trabucho-Alexandre, J., Gröcke, D.R., Uličný, D., Laurin, J., 2015. Intercontinental correlation of organic carbon and carbonate stable isotope records: evidence of climate and sea-level change during the Turonian (Cretaceous). The Depositional Record 1 (2), 53–90.

Jenkyns, H.C., 2010. Geochemistry of oceanic anoxic events. Geochem. Geophys. Geosyst. 11 (3).

Johnsson, M.J., Basu, A., 1993. The system controlling the composition of clastic sediments. Special Papers-Geological society of america.

Kandemir, R., 2004. Gümüşhane ve yakın yörelerindeki erken-orta jura yaşlı şenköy formasyonu'nun çökel özellikleri ve birikim koşulları. Karadeniz Technical University, Trabzon. Turkish, Phd Thesis.

Kandemir, R., Özyurt, M., Karsli, O., 2022. Sedimentological and geochemical characteristics of Lower Jurassic Sandstones from Gümüşhane, NE Turkey: implications for source to sink processes, paleoenvironmental conditions, provenance and tectonic settings. Int. Geol. Rev. 64 (12), 1719–1742.

Kara-Gülbay, R., Kırmacı, M.Z., Korkmaz, S., 2012. Organic geochemistry and depositional environment of the Aptian bituminous limestone in the Kale Gümüşhane area (NE-Turkey): An example of lacustrine deposits on the platform carbonate sequence. Org Geochem. 49, 6–17.

Kılıç, N., 2009. Gümüşhane-Bayburt Yörese Kretase-Tersiyer Geçişinin Foraminifer Ve Sedimantoloji Kayıtları (Kd Türkiye). Karadeniz Technical University. PhD Thesis.

Kırmacı, M.Z., 1992. Sedimentological investigation of the Upper Jurassic–Lower Cretaceous Berdiga Limestone in the Alucra-Gümüşhane-Bayburt regions Eastern Pontides, NE, Turkey. NE, Turkey (Doctoral dissertation, Ph. D. thesis, Karadeniz Technical University, Trabzon (unpublished)(in Turkish with English abstract)).

Kirmaci, M.Z., Koch, R., Bucur, J.I., 1996. An Early Cretaceous section in the Kircaova Area (Berdiga Limestone, NE-Turkey) and its correlation with platform carbonates in W-Slovenia. Facies 34, 1–21.

Kırmacı, M.Z., Yıldız, M., Kandemir, R., Eroğlu-Gümrük, T., 2018. Multistage dolomitization in Late Jurassic-Early Cretaceous platform carbonates (Berdiga Formation), Başoba Yayla (Trabzon), NE Turkey: Implications of the generation of magmatic arc on dolomitization. Mar. Pet. Geol. 89, 515–529.

Koch, R., Bucur, I.I., Kirmaci, M.Z., Eren, M., Tasli, K., 2008. Upper Jurassic and Lower Cretaceous carbonate rocks of the Berdiga Limestone-Sedimentation on an onbound platform with volcanic and episodic siliciclastic influx. Biostratigraphy, facies and. Neues Jahrbuch fur Geologie und Palaontologie-Abhandlungen 247 (1), 23–62.

Koçyiğit, A., Altiner, D., 2002. Tectonostratigraphic evolution of the North Anatolian Palaeorift (NAPR): Hettangian-Aptian passive continental margin of the northern Neo-Tethys, Turkey. Turkish J. Earth Sci. 11 (3), 169–191.

Masse, J.P., Tüysüz, O., Fenerci-Masse, M., Özer, S., Sari, B., 2009. Stratigraphic organisation, spatial distribution, palaeoenvironmental reconstruction, and demise of Lower Cretaceous (Barremian-lower Aptian) carbonate platforms of the Western Pontides (Black Sea region, Turkey). Cretac. Res. 30 (5), 1170–1180.

Nesbitt, H., Young, G.M., 1982. Early Proterozoic climates and plate motions inferred from major element chemistry of lutites. nature 299 (5885), 715–717.

Nesbitt, H.W., Young, G.M., McLennan, S.M., Keays, R.R., 1996. Effects of chemical weathering and sorting on the petrogenesis of siliciclastic sediments, with implications for provenance studies. J. Geol. 104 (5), 525–542.

Okay, A.I., Sahinturk, O., 1997. AAPG Memoir 68: Regional and Petroleum Geology of the Black Sea and Surrounding Region. Chapter 15: Geology of the Eastern Pontides.

Okay, A.I., Tüysüz, O., 1999. Tethyan sutures of northern Turkey. Geol. Soc. Lond. Spec. Publ. 156 (1), 475–515.

Özyurt, M., 2019. Origin of dolomitization in Upper Jurassic-Lower Cretaceous platform carbonates (Berdiga Formation) in the Gümüşhane area PhD. Karadeniz Technical University, Trabzon, Turkey.

Özyurt, M., Hollis, C., 2019. REE+Y characteristics of shallow to deep marine carbonates in Gümüşhane (NE Turkey): Application for paleoenvironmental reconstruction. 34th IAS Meeting of Sedimentology (10-13 Sep 2019, Rome, Italy).

Özyurt, M., Kırmacı, M.Z., under review. Microfacies and geochemistry of Kimmeridgian limestone strata in Eastern Pontide (NE Türkiye): New insight into paleoclimatic and paleoenvironmental conditions. Submitted to Journal of Depositional Records.

Özyurt, M., Kırmacı, M.Z., Al-Aasm, I.S., 2019a. Geochemical characteristics of Upper Jurassic-Lower Cretaceous platform carbonates in Hazine Mağara, Gümüşhane (northeast Turkey): implications for dolomitization and recrystallization. Can. J. Earth Sci. 56 (3), 306–320.

Özyurt, M., Al-Aasm, I.S., Ziya Kirmaci, M., 2019b. Diagenetic Evolution of Upper Jurassic-Lower Cretaceous Berdiga Formation, NE Turkey: Petrographic and Geochemical Evidence. In Paleobiodiversity and Tectono-Sedimentary Records in the Mediterranean Tethys and Related Eastern Areas: Proceedings of the 1st Springer Conference of the Arabian Journal of Geosciences (CAJG-1), Tunisia 2018. Springer International Publishing, pp. 175-177.

Özyurt, M., Ziya Kirmaci, M., Ömer Yılmaz, İ., Kandemir, R., 2019c. Sedimentological and Geochemical Records of Lower Cretaceous Carbonate Successions Around Trabzon (NE Turkey): Implications for Paleoenvironmental Evolution and Paleoclimatological Conditions of Tethys. In *Patterns and Mechanisms of Climate, Paleoclimate and Paleoenvironmental Changes from Low-Latitude Regions: Proceedings of the 1st Springer Conference of the Arabian Journal of Geosciences (CAJG-1), Tunisia 2018*, Springer International Publishing, pp. 19-21.

Özyurt, M., Kırmacı, M.Z., Al-Aasm, I., Hollis, C., Taslı, K., Kandemir, R., 2020. REE characteristics of Lower Cretaceous Limestone Succession in Gümüşhane, NE Turkey: implications for Ocean Paleoredox conditions and diagenetic alteration. Minerals 10 (8), 683.

Özyurt, M., Kırmacı, M.Z., Yılmaz, İ.Ö., Kandemir, R., Taslı, K., 2022. Sedimentological and geochemical approaches for determination of the palaeoceanographic and palaeoclimatic conditions of Lower Cretaceous marine deposits in the eastern part of Sakarya Zone, NE Turkey. Carbonates and Evaporites 37 (2), 25.

Özyurt, M., Kırmacı, M.Z., Al-Aasm, I.S., Kandemir, R., n.d.. (under review) Geochemistry of the massive dolomites in Eastern Black Sea Region: REE implications for dolomite petrogenesis. Submitted to Journal of Geochemistry International.

Özyurt, M., Kırmacı M.Z., Hollis, C., in prep. REE chemistry of glauconite bearing limestone strata (Eastern Pontide, Black Sea Region): New insight into paleoenvironmental conditions.

Pan, Y., Huang, Z., Guo, X., Wang, R., Lash, G.G., Fan, T., Liu, W., 2022. A re-assessment and calibration of redox thresholds in the Permian Lucaogou Formation of the Malang Sag, Santanghu Basin, Northwest China. Mar. Petrol. Geol. 135, 105406.

Pelin, S., 1977. Geological study of the area southeast of Alucra (Giresun) with special reference to its petroleum potential. Karadeniz teknik universitesi, yerbilimleri dergisi, Jeoloji 1, 15–20.

Piper, D.Z., 1974. Rare earth elements in the sedimentary cycle: a summary. Chem. Geol. 14 (4), 285–304.

Qin, Z., Xu, D., Kendall, B., Zhang, X., Ou, Q., Wang, X., Liu, J., 2022. Molybdenum isotope-based redox deviation driven by continental margin euxinia during the early Cambrian. Geochim. Cosmochim. Acta 325, 152–169.

Quinby-Hunt, M.S., Wilde, P., 1994. Thermodynamic zonation in the black shale facies based on iron-manganese-vanadium content. Chem. Geol. 113 (3–4), 297–317.

Roy, D.K., Roser, B.P., 2013. Climatic control on the composition of Carboniferous-Permian Gondwana sediments, Khalaspir basin, Bangladesh. Gondwana Res. 23 (3), 1163–1171.

Sari, B., Kandemır, R., Özer, S., Walaszczyk, I., Görmüş, M., Demırcan, H., Yilmaz, C., 2014. Upper Campanian calciclastic turbidite sequences from the Hacımehmet area (eastern Pontides, NE Turkey): integrated biostratigraphy and microfacies analysis. Acta Geol. Pol. 64 (4), 393–418.

Schlanger, S.O., Jenkyns, H.C., 1976. Cretaceous oceanic anoxic events: causes and consequences. Geol. Mijnb. 55 (3–4).

Taslı, K., 1991. Stratigraphy, paleogeography and micropaleontology of Upper Jurassic–Lower Cretaceous carbonate sequence in the Gümüshane and Bayburt areas (NE Turkey). Unpublished PhD Thesis (in Turkish), Black Sea Technical University, Trabzon, 223pp.

Taslı, K., Özsayar, T., 1997. Stratigraphy and paleoenvironmental setting of the Albian-Campanian deposits within the Gümüßhane province (Eastern Pontides, NE Turkey). Turk. Assoc. Petrol. Geol. Bull 9, 13–29.

Tasli, K., Özer, E., Yilmaz, C., 1999. Biostratigraphic and environmental analysis of the Upper Jurassic-lower cretaceous carbonate sequence in the Başoba Yayla Area (Trabzon, NE Turkey). Turk. J. Earth Sci. 8 (2), 125–135.

Taylor, S.R., McLennan, S.M. 1985. The continental crust: its composition and evolution.

Tribovillard, N., Algeo, T.J., Lyons, T., Riboulleau, A., 2006. Trace metals as paleoredox and paleoproductivity proxies: an update. Chem. Geol. 232 (1–2), 12–32.

Türk-Öz, E., Özyurt, M., 2019. Palaeoenvironment reconstruction and planktonic foraminiferal assemblages of Campanian (Cretaceous) carbonate succession, Çayırbağ area (Trabzon, NE Turkey). Carbonates Evaporites 34, 419–431.

Tüysüz, O., 2018. Cretaceous geological evolution of the Pontides. Geol. Soc. Lond. Spec. Publ. 464 (1), 69–94.

Vincent, S.J., Guo, L., Flecker, R., BouDagher-Fadel, M.K., Ellam, R.M., Kandemir, R., 2018. Age constraints on intra-formational unconformities in Upper Jurassic-Lower Cretaceous carbonates in northeast Turkey; geodynamic and hydrocarbon implications. Mar. Pet. Geol. 91, 639–657.

Wagreich, M., 2012. “ OAE 3”–regional Atlantic organic carbon burial during the Coniacian-Santonian. Clim. Past 8 (5), 1447–1455.

Wang, J.H., Wei, F.I., Chang, Y.S., Shih, H.C., 1997. The corrosion mechanisms of carbon steel and weathering steel in SO2 polluted atmospheres. Mater. Chem. Phys. 47 (1), 1–8.

Wang, J., Cao, Y.C., Wang, X.T., Liu, K.Y., Wang, Z.K., Xu, Q.S., 2018. Sedimentological constraints on the initial uplift of the West Bogda Mountains in Mid-Permian. Sci. Rep. 8 (1), 1–14.

Yakovishina, E.V., Bordunov, S.I., Kopaevich, L.F., Netreba, D.A., Krasnova, E.A., 2022. Climatic Fluctuations and Sedimentation Conditions of the Turonian-Coniacian Sediments of the Northwest Caucasus. Stratigr. Geol. Correl. 30 (3), 147–166.

Yandoka, B.M.S., Abdullah, W.H., Abubakar, M.B., Hakimi, M.H., Adegoke, A.K., 2015a. Geochemical characterisation of Early Cretaceous lacustrine sediments of Bima Formation, Yola Sub-basin, Northern Benue Trough, NE Nigeria: Organic matter input, preservation, paleoenvironment and palaeoclimatic conditions. Mar. Pet. Geol. 61, 82–94.

Yandoka, B.M.S., Abubakar, M.B., Abdullah, W.H., Maigari, A.S., Hakimi, M.H., Adegoke, A.K., Aliyu, A.H., 2015b. Sedimentology, geochemistry and paleoenvironmental reconstruction of the Cretaceous Yolde formation from Yola Sub-basin, Northern Benue Trough, NE Nigeria. Mar. Pet. Geol. 67, 663–677.

Yilmaz, C., Kandemir, R., 2006. Sedimentary records of the extensional tectonic regime with temporal cessation: Gumushane Mesozoic Basin (NE Turkey). Geologica Carpathica-Bratislava 57 (1), 3.

Yilmaz, I.O., Altiner, D., Tekin, U.K., Tuysuz, O., Ocakoglu, F., Acikalin, S., 2010. Cenomanian-Turonian Oceanic Anoxic Event (OAE2) in the Sakarya Zone, northwestern Turkey: sedimentological, cyclostratigraphic, and geochemical records. Cretac. Res. 31 (2), 207–226.

Yıldızoğlu, S., 2022. Sedimentological and geochemical properties of the Kindiralik Dere Formation, Gümüşhane, Türkiye, Master Thesis. Recep Tayyip Erdoğan University.

Zatoń, M., Marynowski, L., Szczepanik, P., Bond, D.P., Wignall, P.B., 2009. Redox conditions during sedimentation of the Middle Jurassic (Upper Bajocian–Bathonian) clays of the Polish Jura (south-central Poland). Facies 55, 103–114.

Zhang, X., Chen, K., Hu, D., Sha, J., 2016. Mid-Cretaceous carbon cycle perturbations and Oceanic Anoxic Events recorded in southern Tibet. Sci. Rep. 6 (1), 39643.